Position Estimation in a True Asymmetric Cascade H-Bridge Multilevel Inverter

Kamel Saleh, Mark Sumner
An-Najah National University Palestine, University of Nottingham UK.
E-Mail: kamel.saleh@najah.edu

Keywords

«Sensorless», «Multilevel converter», «2-Level Converter», «SVPWM».

Abstract

This paper introduces a new method to track the saliency of motor fed by a multilevel inverter through measuring the dynamic current response of the motor line currents due the IGBT switching actions. The method uses only the fundamental PWM waveform (i.e there is no modification to the operation of the multilevel inverter) similar to the fundamental PWM method proposed for a 2-level inverter. Simulation results are provided to demonstrate the performance of the complete sensorless speed control of a PM motor driven by such a converter over a wide speed range. Finally the paper introduces a comparison between the 2-level inverter and the multilevel inverter in terms of the reduction of the Total Harmonic Distortion (THD) using the fundamental PWM method in both cases.

Introduction

Sensorless control of motor drives using two level inverters has been widely researched for systems employing standard two level inverters. At low and zero speed, some form of additional excitation has been proposed, such as the injection of a high frequency (HF) voltage or current [1-3] or the injection of test pulses [4-6]. However, these techniques introduce significant additional current distortion either due to the injected signals themselves (as in the HF injection methods and the INFORM method [4]) or due to the insertion of the minimum pulse width in the operation of the drive system when applying the Fundamental PWM Excitation method (FPE) [6].This distortion causes audible noise, torque pulsations and increases the system losses.

The multilevel converter can achieve a higher voltage and power capability with conventional switching devices compared to two level converters, and is now used for high power drives [7]. Multilevel converters employ switching devices connected in a chain, which sequentially switch different DC voltages across the motor using a specialist PWM technique, to create a stepped output voltage. The particular structure of some of these converters offers significant potential for improving sensorless control of motors, as they employ H bridge circuits with a relatively low DC link voltage. [8] uses H-Bridges connected in series with 2-Level inverter which are used to generate a small voltage pluses used only to track the saliency position, this technique achieve a good sensorless results at the same time reduce significantly the current distortion due to the use of small voltage pulses. Previous research into sensorless multilevel drives used a special multilevel topology where the H-Bridges were used only for generating the voltage pulses to track the saliency [9], and were added to a conventional 2-level converter. In this paper a new technique is proposed to track the saliency in any motor driven by any multilevel inverter topology without disturbing the operation of the multilevel inverter. At the same time it reduces the current distortion associated with the 2-Level sensorless techniques significantly through making use of the small voltage steps of the multilevel inverter output as an excitation voltages.

Position Estimation in an Asymmetric Hybrid Cascade H-Bridge Inverter

Fig 1.a shows the Asymmetric Cascade H-Bridge Inverter topology [7] used in high power applications. The first set of H-Bridges have a higher DC link voltage (2V), and employ GTOs or

IGCTs as switching devices which are controlled at relatively low frequency. The second set of H-Bridges have a lower DC link voltage (V) and employ IGBTs with a higher switching frequency. This arrangement meets with the characteristics of both the IGBTs and GTOs. Using an asymmetric DC link voltage helps to generate 7 level voltages from 2 H-Bridges only as shown in Fig 1.b.

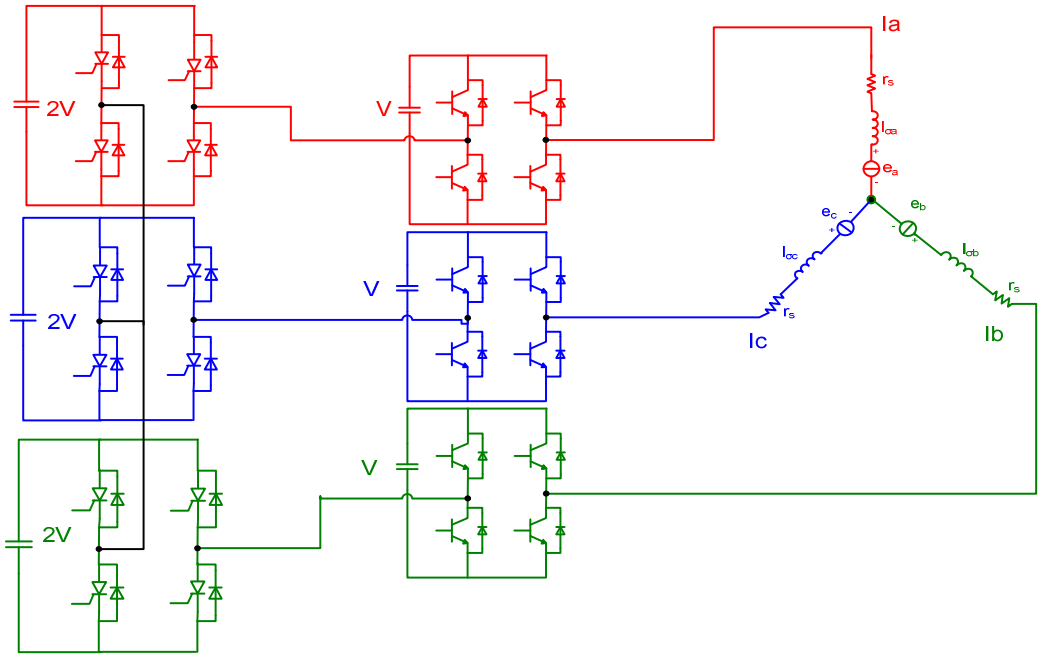

Fig 1.a 7-Level Asymmetric Hybrid H-Bridge Converter Topology

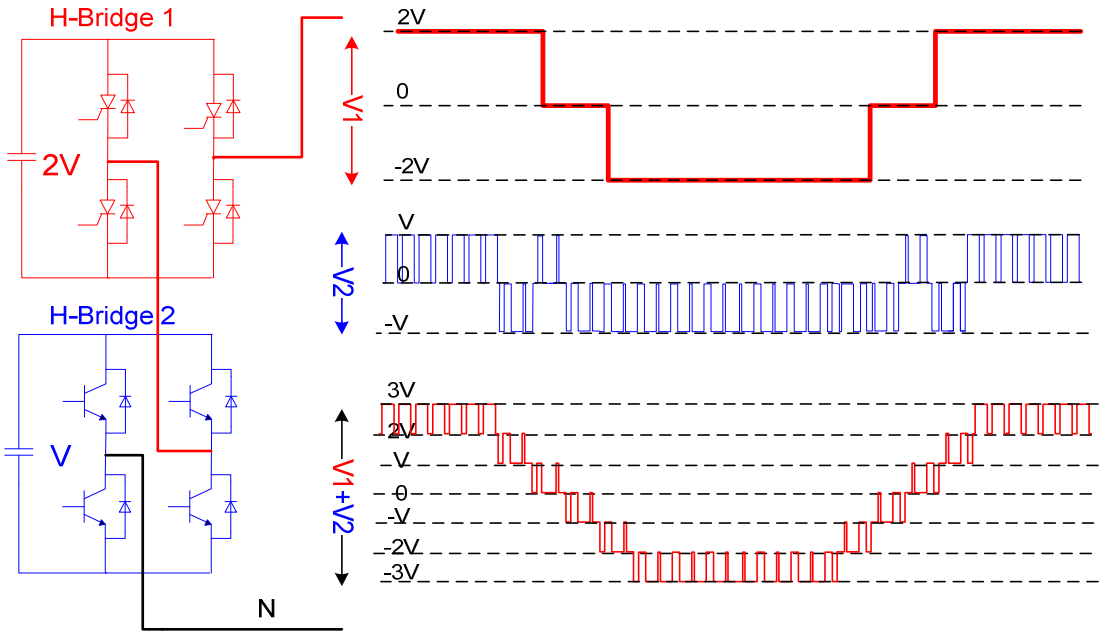

Fig 1.b Operation of the seven level asymmetric hybrid cascaded H-bridge converter.

Space vector modulation for multilevel inverters has been widely researched [9],[10],[11]. Many techniques were proposed in order to simplify the process of choosing the switching sequence from many switching sequences available in multilevel inverter. In this paper the space vector modulation technique illustrated in [9] has been adopted. Fig 2 shows the first sector of the space vector modulation state diagram for 7-level inverter. If V_ref exists in any triangle in the first sector, then the

switching sequences and the timing of the applied vectors will be one of the four switching sequences shown in Fig 2 according to triangle where V_ref exists. The way to identify the triangle and hence to choose the correct switching sequence ie Type0,Type1,Type2 and Type 3 is clarified in [9].

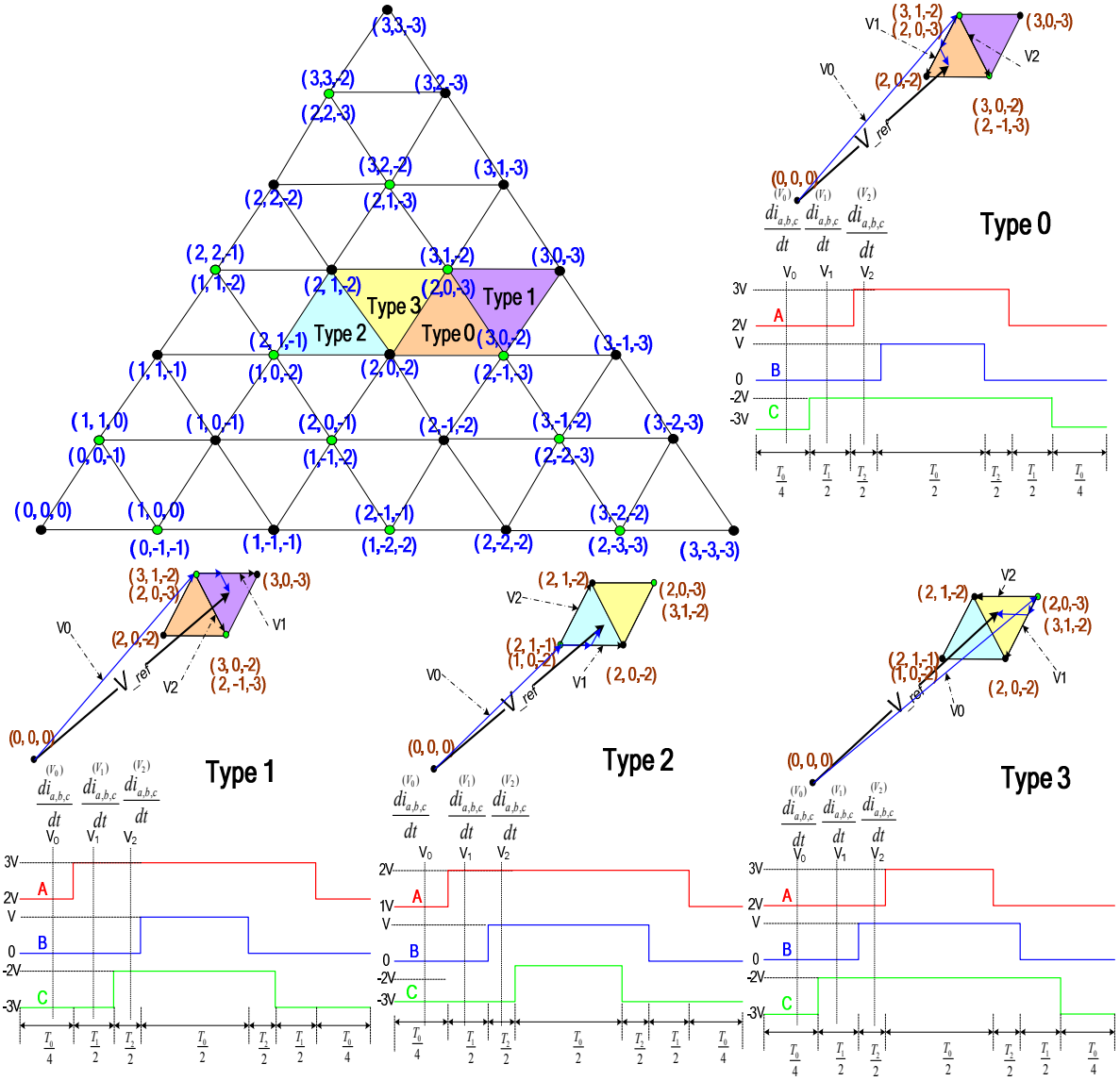

Fig 2. Sector 1 of a 7 level Space Vector state diagram and its different switching sequences.

Tracking the Saliency in Multilevel Inverter

It is possible to track the saliency using the PWM signals in a multilevel inverter in similar way to that introduced in [6] for a 2-level inverter without interrupting the multilevel inverter normal operation because of the test vectors. Fig 3 shows the Type0 switching sequence .The stator circuit when the vectors V1, V2 and V0 are applied are shown in Fig 4.a, 4.b and 4.c respectively.

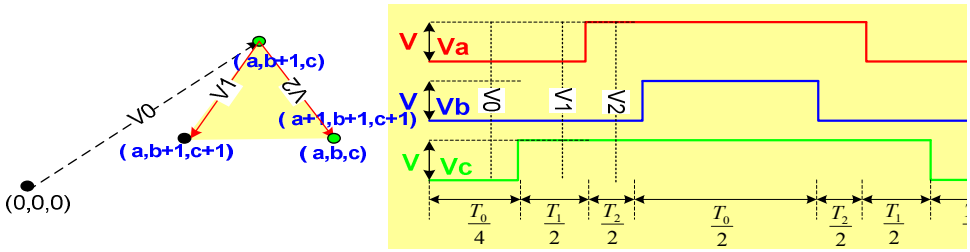

Fig 3 Switching sequence for Type0 in sector 1 in the multilevel space diagram.

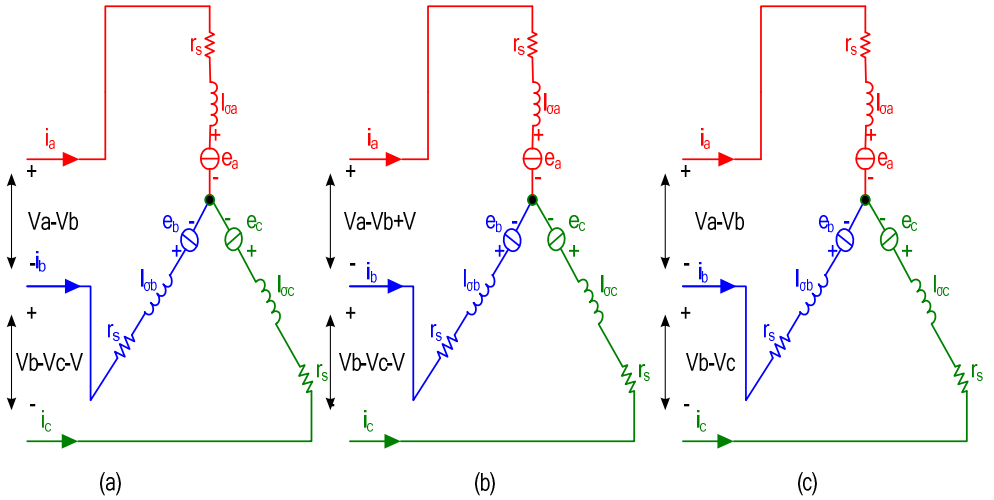

Fig 4 Stator circuits when: (a) V1 is applied; (b) V2 is applied; (c) V0 is applied.

Using the circuit in Fig 4.a, the following equations hold true:-

$$Va - Vb = l_{\sigma a} * \frac{di_a^{(V1)}}{dt} - l_{\sigma b} * \frac{di_b^{(V1)}}{dt} \quad (1)$$

$$\mathrm{Vb} - \mathrm{Vc} - \mathrm{V} = l_{\sigma b} * \frac{di_b^{(V1)}}{dt} - l_{\sigma c} * \frac{di_c^{(V1)}}{dt} \quad (2)$$

$$Vc - Va + V = l_{\sigma c} * \frac{di_c^{(V1)}}{dt} - l_{\sigma a} * \frac{di_a^{(V1)}}{dt} \quad (3)$$

The following equations are obtained using Fig 4.b:-

$$Va - Vb + V = l_{\sigma a} * \frac{di_a^{(V2)}}{dt} - l_{\sigma b} * \frac{di_b^{(V2)}}{dt} \quad (4)$$

$$\mathrm{Vb} - \mathrm{Vc} - \mathrm{V} = l_{\sigma b} * \frac{di_b^{(V2)}}{dt} - l_{\sigma c} * \frac{di_c^{(V2)}}{dt} \quad (5)$$

$$Vc - Va = l_{\sigma c} * \frac{di_c^{(V2)}}{dt} - l_{\sigma a} * \frac{di_a^{(V2)}}{dt} \quad (6)$$

Finally when V0 is applied as shown in Fig 4.c, the following equations hold true:-

$$Va - Vb = l_{\sigma a} * \frac{di_a^{(V0)}}{dt} - l_{\sigma b} * \frac{di_b^{(V0)}}{dt} \quad (7)$$

$$\mathrm{Vb} - \mathrm{Vc} = l_{\sigma b} * \frac{di_b^{(V0)}}{dt} - l_{\sigma c} * \frac{di_c^{(V0)}}{dt} \quad (8)$$

$$Vc - Va = l_{\sigma c} * \frac{di_c^{(V0)}}{dt} - l_{\sigma a} * \frac{di_a^{(V0)}}{dt} \quad (9)$$

All the above equations are obtained based on two assumptions. The first one is that the voltage drop across the stator resistances are small and can be neglected. The second one is that back emf can be cancelled if the time separation between the vectors is small.

Subtracting (7, 8 and 9) from (4, 5 and 6) respectively yields:-

$$0 = l_{\sigma a} * (\frac{di_a^{(V1)}}{dt} - \frac{di_a^{(V0)}}{dt}) - l_{\sigma b} * (\frac{di_b^{(V1)}}{dt} - \frac{di_b^{(V0)}}{dt}) \quad (10)$$

$$-V = l_{\sigma b} * \left(\frac{di_b^{(V1)}}{dt} - \frac{di_b^{(V0)}}{dt}\right) - l_{\sigma c} * (\frac{di_c^{(V1)}}{dt} - \frac{di_c^{(V0)}}{dt}) \quad (11)$$

$$V = l_{\sigma c} * \left(\frac{di_c^{(V1)}}{dt} - \frac{di_c^{(V0)}}{dt}\right) - l_{\sigma a} * (\frac{di_a^{(V1)}}{dt} - \frac{di_a^{(V0)}}{dt}) \quad (12)$$

Repeating the previous procedure with equations (1, 2 and 3) gives:-

$$V = l_{\sigma a} * (\frac{di_a^{(V2)}}{dt} - \frac{di_a^{(V0)}}{dt}) - l_{\sigma b} * (\frac{di_b^{(V2)}}{dt} - \frac{di_b^{(V0)}}{dt}) \quad (13)$$

$$-V = l_{\sigma b} * \left(\frac{di_b^{(V2)}}{dt} - \frac{di_b^{(V0)}}{dt}\right) - l_{\sigma c} * (\frac{di_c^{(V2)}}{dt} - \frac{di_c^{(V0)}}{dt}) \quad (14)$$

$$0 = l_{\sigma c} * \left(\frac{di_c^{(V2)}}{dt} - \frac{di_c^{(V0)}}{dt}\right) - l_{\sigma a} * (\frac{di_a^{(V2)}}{dt} - \frac{di_a^{(V0)}}{dt}) \quad (15)$$

Multiplying (10) by $(l_{\sigma c})$, (11) by $(l_{\sigma a})$ and (12) by $(l_{\sigma b})$ and then subtracting the new equations from each other yields:-

$$-l_{\sigma b} * V = \left(\frac{di_a^{(V1)}}{dt} - \frac{di_a^{(V0)}}{dt}\right)(l_{\sigma a}\, l_{\sigma b} + \, l_{\sigma b} l_{\sigma c} + l_{\sigma c} l_{\sigma a}) \quad (16)$$

$$-l_{\sigma a} * V = \left(\frac{di_b^{(V1)}}{dt} - \frac{di_b^{(V0)}}{dt}\right)(l_{\sigma a}\, l_{\sigma b} + \, l_{\sigma b} l_{\sigma c} + l_{\sigma c} l_{\sigma a}) \quad (17)$$

$$(l_{\sigma a} + l_{\sigma b}) * V \; = \left(\frac{di_c^{(V1)}}{dt} - \frac{di_c^{(V0)}}{dt}\right)(l_{\sigma a}\, l_{\sigma b} + \, l_{\sigma b} l_{\sigma c} + l_{\sigma c} l_{\sigma a}) \quad (18)$$

Substituting $l_{\sigma a}\, l_{\sigma b} + \, l_{\sigma b} l_{\sigma c} + l_{\sigma c} l_{\sigma a}$ by $3L_0(1 - \left(\frac{\Delta L}{2L_0}\right)^2)$ yields:

$$\left(\frac{di_a^{(V1)}}{dt} - \frac{di_a^{(V0)}}{dt}\right) = \frac{-V * l_{\sigma b}}{3L_0(1-\left(\frac{\Delta L}{2L_0}\right)^2)} \quad (19)$$

$$\left(\frac{di_b^{(V1)}}{dt} - \frac{di_b^{(V0)}}{dt}\right) = \frac{-V * l_{\sigma a}}{3L_0(1-\left(\frac{\Delta L}{2L_0}\right)^2)} \quad (20)$$

$$\left(\frac{di_c^{(V1)}}{dt} - \frac{di_c^{(V0)}}{dt}\right) = \frac{V * (l_{\sigma a} + l_{\sigma b})}{3L_0(1-\left(\frac{\Delta L}{2L_0}\right)^2)} \quad (21)$$

By assuming a constant $C = \frac{3(1-\left(\frac{\Delta L}{2L_0}\right)^2)}{V}$, (19, 20 and 21) can be rearranged for the position signals:-

$$Pa = -1 - C\left(\frac{di_b^{(V1)}}{dt} - \frac{di_b^{(V0)}}{dt}\right) \quad (22)$$

$$Pb = -1 - C\left(\frac{di_a^{(V1)}}{dt} - \frac{di_a^{(V0)}}{dt}\right) \quad (23)$$

$$Pc = 2 - C\left(\frac{di_c^{(V1)}}{dt} - \frac{di_c^{(V0)}}{dt}\right) \quad (24)$$

In the same way (13, 14 and 15) yields:-

$$Pa = -1 + C\left(\frac{di_c^{(V2)}}{dt} - \frac{di_c^{(V0)}}{dt}\right) \quad (25)$$

$$Pb = 2 + C\left(\frac{di_b^{(V2)}}{dt} - \frac{di_b^{(V0)}}{dt}\right) \quad (26)$$

$$Pc = -1 + C\left(\frac{di_a^{(V1)}}{dt} - \frac{di_a^{(V0)}}{dt}\right) \quad (27)$$

Comparing these equations to the positional equations obtained in table 1 (position equation obtained using SVPWM in a 2 level inverter) [6], it is quite clear that (22, 23 and 24) are exactly the same as those obtained by applying vectors V_5 and V_0 in table 1. Also (25, 26 and 27) are exactly the same as those obtained by applying V_6 and V_0 in table 1.

	p_a	p_b	p_c
V_1+V_0	$2-c(\frac{di_a^{(V1)}}{dt}-\frac{di_a^{(V0)}}{dt})$	$-1-c(\frac{di_c^{(V1)}}{dt}-\frac{di_c^{(V0)}}{dt})$	$-1-c(\frac{di_b^{(V1)}}{dt}-\frac{di_b^{(V0)}}{dt})$
V_2+V_0	$-1+c(\frac{di_b^{(V2)}}{dt}-\frac{di_b^{(V0)}}{dt})$	$-1+c(\frac{di_a^{(V2)}}{dt}-\frac{di_a^{(V0)}}{dt})$	$2+c(\frac{di_c^{(V2)}}{dt}-\frac{di_c^{(V0)}}{dt})$
V_3+V_0	$-1-c(\frac{di_c^{(V3)}}{dt}-\frac{di_c^{(V0)}}{dt})$	$2-c(\frac{di_b^{(V3)}}{dt}-\frac{di_b^{(V0)}}{dt})$	$-1-c(\frac{di_a^{(V3)}}{dt}-\frac{di_a^{(V0)}}{dt})$
V_4+V_0	$2+c(\frac{di_a^{(V4)}}{dt}-\frac{di_a^{(V0)}}{dt})$	$-1+c(\frac{di_c^{(V4)}}{dt}-\frac{di_c^{(V0)}}{dt})$	$-1+c(\frac{di_b^{(V4)}}{dt}-\frac{di_b^{(V0)}}{dt})$
V_5+V_0	$-1-c(\frac{di_b^{(V5)}}{dt}-\frac{di_b^{(V0)}}{dt})$	$-1-c(\frac{di_a^{(V5)}}{dt}-\frac{di_a^{(V0)}}{dt})$	$2-c(\frac{di_c^{(V5)}}{dt}-\frac{di_c^{(V0)}}{dt})$
V_6+V_0	$-1+c(\frac{di_c^{(V6)}}{dt}-\frac{di_c^{(V0)}}{dt})$	$2+c(\frac{di_b^{(V6)}}{dt}-\frac{di_b^{(V0)}}{dt})$	$-1+c(\frac{di_a^{(V6)}}{dt}-\frac{di_a^{(V0)}}{dt})$

Table1 Selection of pa, pb and pc for a star-connected machine with a 2 level SVPWM.

This result can be understood by imagining that the Type 0 triangle in Fig 2 is similar to sector 5 in a 2 level SVPWM switching state diagram. Also the active vectors V1 and V2 in the multilevel SVPWM switching sequence in this example are similar to V5 and V6 respectively of the 2-level SVPWM switching sequence. Based on that the scalar position equations for Type1,Type2 and Type 3 triangles in sector 1 for multilevel SVPWM switching state diagram will be the same as those obtained for sector 6, sector 1, and sector 4 in 2-level SVPWM switching state diagram as shown in Table2. One point should be taken in consideration is that this table is correct in sector 1 only. In other sectors the triangles Type0 ,Type1, Type2 and Type 3 will no longer be similar to sector 5, sector 6, sector1 and

sector 4 of the 2-level switching state diagram and so the position scalar equations will be slightly different but still can be deduced directly from Table 1 as the only change will be the sector that the triangle will be similar to. For example, Type 0 is similar to sector 5 if V_ref exists in sector 1 of the multilevel inverter SVPWM switching state diagram. And it will be similar to sector 1 if V_ref exists in sector 3 of the multilevel SVPWM switching state diagram as shown in Fig 5. Hence the scalar position equations will be chosen from table 1 accordingly.

Triangle	Vectors	Pa	Pb	Pc
Type0 ΔBCD	V1+Vo	$-1-c(\frac{^{(V5)}di_b}{dt}-\frac{^{(V0)}di_b}{dt})$	$-1-c(\frac{^{(V5)}di_a}{dt}-\frac{^{(V0)}di_a}{dt})$	$2-c(\frac{^{(V5)}di_c}{dt}-\frac{^{(V0)}di_c}{dt})$
	V2+Vo	$-1+c(\frac{^{(V6)}di_c}{dt}-\frac{^{(V0)}di_c}{dt})$	$2+c(\frac{^{(V6)}di_b}{dt}-\frac{^{(V0)}di_b}{dt})$	$-1+c(\frac{^{(V6)}di_a}{dt}-\frac{^{(V0)}di_a}{dt})$
Type1 ΔBCA	V1+Vo	$2-c(\frac{^{(V1)}di_a}{dt}-\frac{^{(V0)}di_a}{dt})$	$-1-c(\frac{^{(V1)}di_c}{dt}-\frac{^{(V0)}di_c}{dt})$	$-1-c(\frac{^{(V1)}di_b}{dt}-\frac{^{(V0)}di_b}{dt})$
	V2+Vo	$-1+c(\frac{^{(V6)}di_c}{dt}-\frac{^{(V0)}di_c}{dt})$	$2+c(\frac{^{(V6)}di_b}{dt}-\frac{^{(V0)}di_b}{dt})$	$-1+c(\frac{^{(V6)}di_a}{dt}-\frac{^{(V0)}di_a}{dt})$
Type 2 ΔBCD	V1+Vo	$2-c(\frac{^{(V1)}di_a}{dt}-\frac{^{(V0)}di_a}{dt})$	$-1-c(\frac{^{(V1)}di_c}{dt}-\frac{^{(V0)}di_c}{dt})$	$-1-c(\frac{^{(V1)}di_b}{dt}-\frac{^{(V0)}di_b}{dt})$
	V2+Vo	$-1+c(\frac{^{(V2)}di_b}{dt}-\frac{^{(V0)}di_b}{dt})$	$-1+c(\frac{^{(V2)}di_a}{dt}-\frac{^{(V0)}di_a}{dt})$	$2+c(\frac{^{(V2)}di_c}{dt}-\frac{^{(V0)}di_c}{dt})$
Type 3 ΔBCA	V1+Vo	$-1-c(\frac{^{(V1)}di_b}{dt}-\frac{^{(V0)}di_b}{dt})$	$-1-c(\frac{^{(V1)}di_a}{dt}-\frac{^{(V0)}di_a}{dt})$	$2-c(\frac{^{(V1)}di_c}{dt}-\frac{^{(V0)}di_c}{dt})$
	V2+Vo	$2+c(\frac{^{(V2)}di_a}{dt}-\frac{^{(V0)}di_a}{dt})$	$-1+c(\frac{^{(V2)}di_c}{dt}-\frac{^{(V0)}di_c}{dt})$	$-1+c(\frac{^{(V2)}di_b}{dt}-\frac{^{(V0)}di_b}{dt})$

Table2 Selection of pa, pb and pc for a star-connected machine with a multilevel SVPWM.

Fully Sensorless Speed Control

The position and speed control for a PM machine have been implemented in simulation in the Saber modeling environment. The estimated position signals Pαβ from the equations selected, are used as the input to a mechanical observer [12] to obtain the speed $\omega^{\wedge}$ and a "cleaned" position $\theta^{\wedge}$. Note the simulation includes a minimum pulsewidth of 10us when di/dt measurements are made – a realistic values seen from experimental results of [6,9]. This estimated speed $\omega^{\wedge}$ and position $\theta^{\wedge}$ are used to obtain a fully sensorless speed control as shown in Fig 6.

Figure 7 shows the results of full sensorless speed control under no load and full loaded conditions using the proposed method. In Fig 7.a a speed step change from 0 to 15rpm to -15rpm back to 0 rpm at full load was demanded. The measured speed and position seen in the figure proved that the system responded to the speed steps with good dynamic response and good steady state behaviour. One of the

advantages of this method is that its ability to work in sensorless mode over a wide speed range as all the di/dt signals are sample in one PWM period and hence the effect of the back EMF will be very small even at high speed. This is shown Fig 7.b where the motor responded to a speed steps between 0 to 2000 rpm at no load. The performance of the system in this case is good.

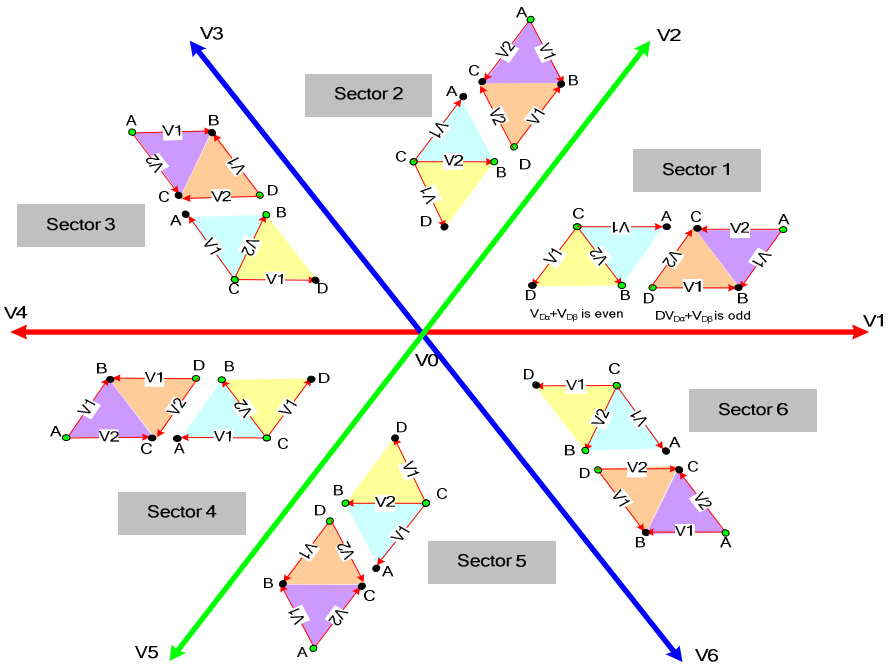

Fig 5 Change of the way the switching sequence is defined in different sectors when using multilevel SVPWM.

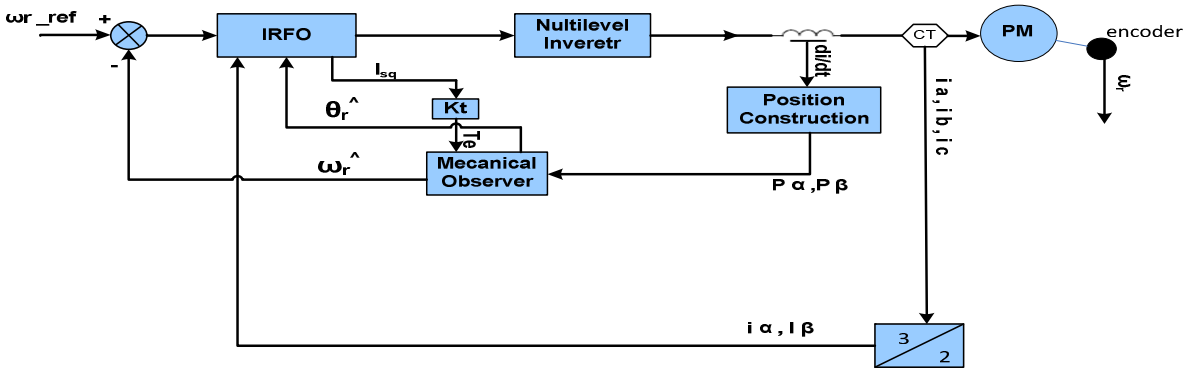

Fig 6 Simulation System used to verify full sensorless speed control.

Improvement in Current Distortion

A comparison is now made between the total harmonic distortion due to the minimum pulse width introduced to the requirements of the di/dt sampling, when implementaon on both a multilevel inverter and a 2-level inverter. The minimum pulse width in both inverters were chosen to be 10µs. the switching frequency is 5kHz, the position is sampled every 4 PWM periods. Fig 8 shows the current waveforms for both the 2-level inverter and multilevel inverter operating at 30 rpm and no load with and without pulse extension. Form the current waveform it is quite clear the improvement in the distortion due to the used of small voltage steps for excitations in the case of multilevel inverter. This improvement is quantified using the THD as shown in table 3.

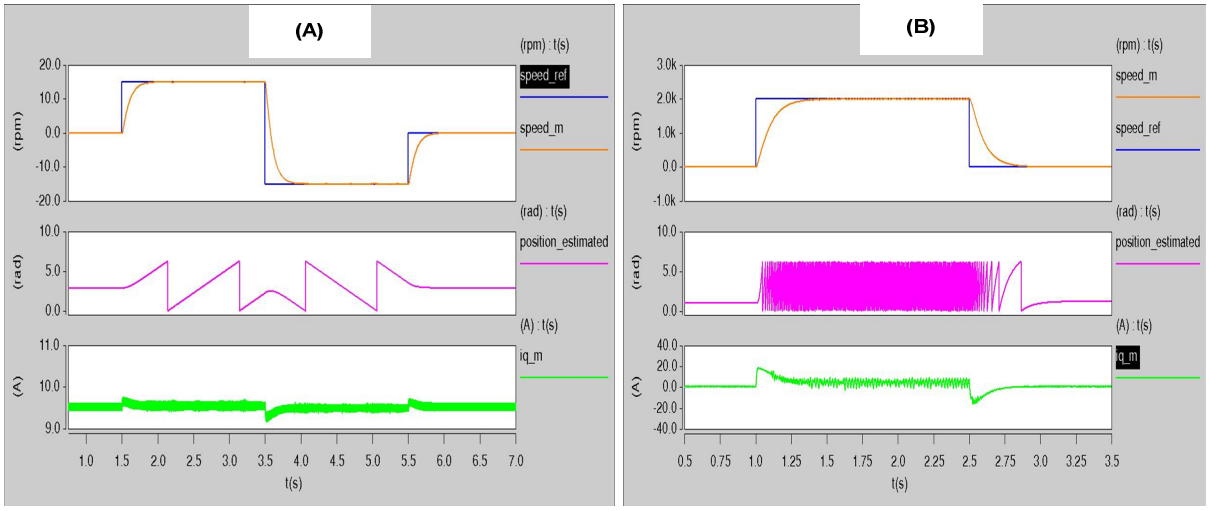

Fig 7.a Fully Sensorless Speed Steps between 0,15,-15 and 0 rpm at full load ,7.b Fully Sensorless Speed Steps between 0,2000, and 0 rpm at no load

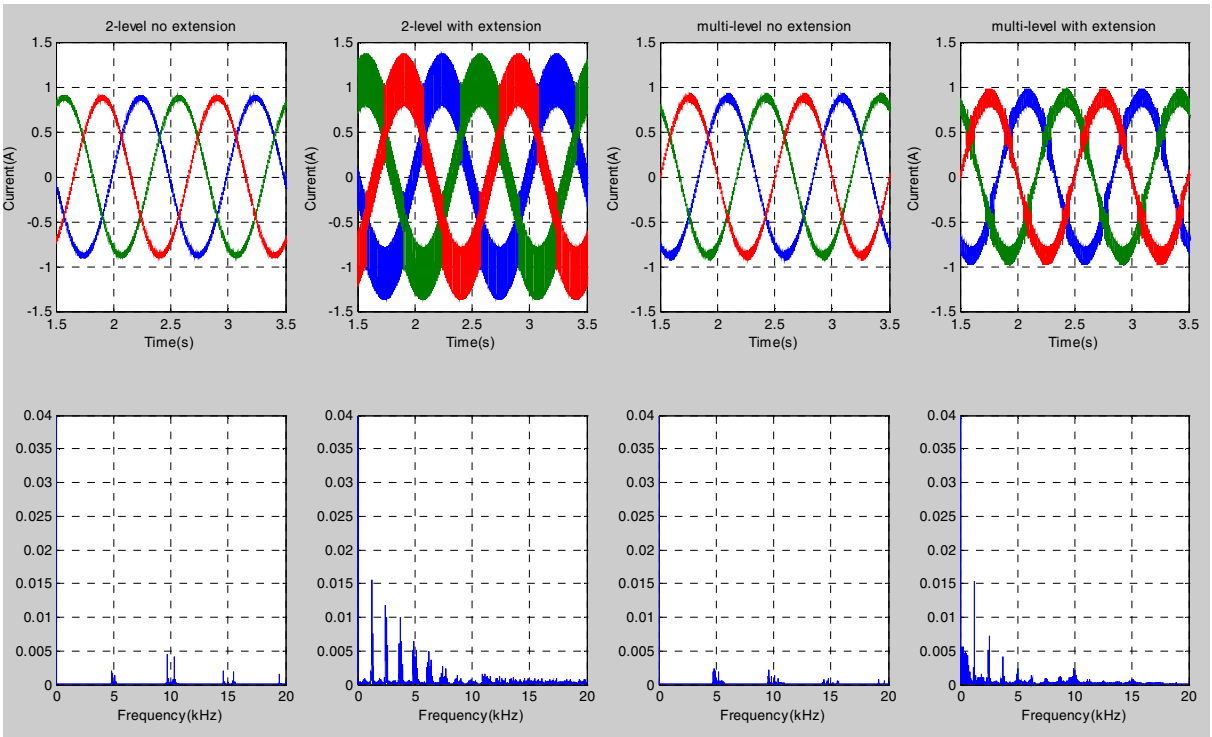

Fig 8 Current waveforms and FFT in 2-level inverter and multilevel inverter at 30 rpm and no load.

Case	2-level , no extension	2-level , with extension	Multi-level, no extension	Multi-level, with extension
THD	2.2%	19.33%	2.167%	7.47%

Table 3 Total Harmonic Distortion in 2-level inverter and multilevel inverter in normal operation and when introducing Tmin to the operation as well.

Conclusion

This paper has outlined a new scheme for tracking the saliency in ac machines driven by a multilevel inverter using the current transient response due multilevel-inverter switching actions without any need to include additional excitation voltages and without any modification to the normal operation of the multilevel inverter. The equations to track the saliency will be similar to those in 2-level inverter [3]. The new method helps to reduce the current distortion significantly compared to the standard 2-level inverter due to the reduction in excitation voltage. The method can be also implemented to different multilevel topologies such as the diode clamped multilevel inverter and can track both the saturation saliency and the rotor slotting saliency.

References

[1] P.L. Jansen, R.D. Lorenz, "Transducerless Position and Velocity Estimation in Induction and Salient AC Machines", IEEE Transactions on Industry Applications, vol.31, pages:240–247, Mar, 1995.

[2] J.-I. Ha, M. Ohto, J.-H. Jang, S.-K. Sul," Design and Selection of AC Machines for Saliency-Based Sensorless Control", Industrial Applications Conference of IEEE, IAS Annual Meeting, vol.2, pages:1155–1162, 2000.

[3] M. Linke, R. Kennel, J. Holtz, "Sensorless Speed and Position Control of Synchronous Machines using Alternating Carrier Injection", IEEE International Electric Machines and Drives Conference IEMDC03, vol.2, pages:1211–1217, 2003.

[4] M. Schroedl. "Sensorless Control of AC Machines at Low Speed and Standstill Based on the INFORM Method". IEEE IAS Annual Meeting, volume 4, pp. 270-277, (1996).

[5] J. Holtz, J. Juliet."Sensorless Acquisition of the Rotor Position Angle of Induction Motors With Arbitrary Stator Windings". IAS Annual Meeting, volume 2, pp.1675-1682, (2004).

[6] G. Qiang, G.M. Asher, M. Sumner, P. Makys. "Position Estimation of AC Machines at all Frequencies Using Only Space Vector PWM based Excitation", 3rd IET International Conference, pp. 61-70, (2006).

[7] M.D.Manjrekar, P.K.Steimer, T.A.Lipo," Hybrid Multilevel Power Conversion System: A competitive Solution for High-Power Applications**"**, IEEE transactions on industry applications, volume 36, pp 834 – 841, (2000)

[8] Sanmin Wei, Bin Wu, Qianghua Wang , "An Improved Space Vector PWM Control Algorithm for Multilevel Inverters**",** Power Electronics and Motion Control Conference, vol.3 ,pages:1124-1129, Aug, 2004.

[9] K. Saleh, G.M. Asher, M. Sumner, M. Tomasini, G. Qiang. "Low Speed Sensorless Control of an Induction Motor Fed by Multilevel Converter to Reduce Current Distortion", EPE 2009 in Barcelona.

[10] B.P. McGrath, D.G.Holmes, T.A Lipo, "Optimised space vector switching sequences for multilevel inverters", Applied Power Electronics Conference and Exposition, 2001. APEC 2001. Sixteenth Annual IEEE, vol. 2, no. 2, pp. 1123 -1129, 2001.

[11] M.M. Prats, L.G. Franquelo, R. Portillo, J.I. Leon, E. Galvan,J.M. Carrasco, "A 3-D space vector modulation generalized algorithm for multilevel converters", Power Electronics Letters, IEEE, vol. 1, no. 4, pp. 110 - 114, 2003.

[12] R.D. Lorenz , K.W. Van Patten. "High-Resolution Velocity Estimation for All-Digital, ac Servo Drives" , IEEE transactions on industry applications, volume 27, pp.701 – 705, (1991).